# Chemotherapuetic Treatment Using Controlled Drug Delivery of BCNU via Nanoparticles

BEE 4530: Computer Aided Engineering – Applications to Biomedical Processes

Group 6:
Matt Brendel
Molly Casey
Rachel Gilbert
Mel Spinella

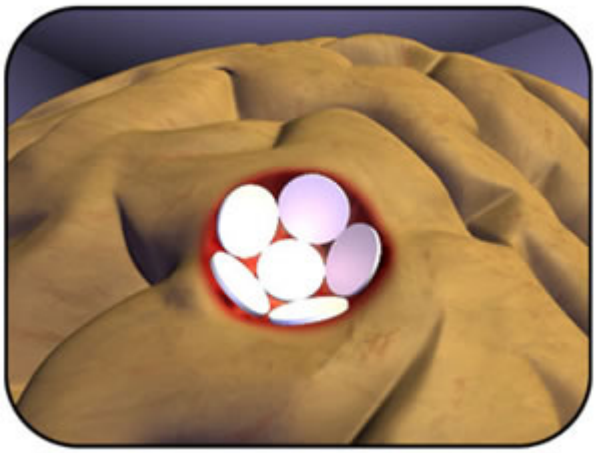

# Contents


I. Executive Summary ..... 3
II. Introduction ..... 4
IIA. Design Objectives: ..... 5
IIB. Problem Schematic: ..... 5
III. Results ..... 6
IV. Mesh Convergence ..... 11
V. Accuracy Check ..... 12
i. Pressure ..... 12
a) Pressure in Cavity ..... 13
b) Pressure in Tumor Layer ..... 13
c) Pressure in Normal Tissue ..... 14
d) Pressure Conclusions ..... 14
ii. Velocity ..... 14
iii. Concentration ..... 16
VI. Sensitivity Analysis ..... 17
i. Edema Length ..... 17
ii. Initial Concentration of Nanoparticles in the Wafers ..... 19
iii. Initial Concentration of BCNU within each Nanoparticle ..... 20
iv. Diffusivity of Nanoparticles ..... 20
VII. Conclusions ..... 21
VIII. Design Recommendations ..... 21
IX. Appendix A: Model Design ..... 23
Governing equations: ..... 23
i. For Diffusion of Nanoparticles: ..... 23
ii. For Diffusion of BCNU: ..... 23
iii. For Convection using Brinkman Equation: ..... 23
Boundary Conditions: ..... 23
i. For Diffusion of Nanoparticles: ..... 23
ii. For Diffusion of BCNU: ..... 23
iii. For Convection: ..... 23
Initial Conditions: ..... 24
i. For Diffusion of Nanoparticles: ..... 24
ii. For Diffusion of BCNU: ..... 24
iii. For Convection: ..... 24
X. Appendix B: Calculations ..... 25
XI. Appendix C: Variables ..... 29
XII. Appendix D: Supplementary Graphs, Tables, and Figures ..... 32
IX. Appendix E: References ..... 36

## I. Executive Summary

The most common type of brain tumor is the glioma and despite advances in diagnostic imaging and drug delivery, there are no effective cures. This is due to the malignant glioma's tendency to recur after treatment, with the recurrence being within a 4cm region from the edge at which it was surgically removed. However, local delivery mechanisms have provided a way for drug to reach the malignant tumors directly. One of these mechanisms is the use of the drug BCNU that is inserted into the cavity via dissolvable Gliadel wafers. These wafers have shown the ability to provide high drug concentrations to a localized area, but at a limited penetration distance of 1 to 2 cm. Consequently, our objective is to improve the design of the Gliadel wafer by encapsulating the BCNU in nanoparticles consisting of PSA with the goal that these nanoparticles will diffuse far enough from the wafers that the drug will reach a higher penetration distance.

The drug delivery was modeled in COMSOL, using three governing equations: one to model the diffusion of the nanoparticles from the wafer into the tissue, one to model the diffusion of the drug out of the nanoparticles into the tissue, and another to model interstitial fluid flow in the brain. An axisymmetric cylindrical geometry was used to model the entire complex. The concentration of the BCNU out of the nanoparticles was modeled proportionally to the volume of the nanoparticle that was degraded. To accurately model drug delivery, interstitial fluid flow was taken into account due to its ability to cause a significant convective flux for the transport of macromolecules.

The simulation was run for 12 days and a distance of 4cm from the removed tumor was reached above the therapeutic value of $5.394 \times 10^{-12}$ mg/mm$^3$. This was then compared to the method of BCNU delivery directly from the Gliadel wafers which are in the absence of nanoparticles. The results show that upon reaching the threshold value, the wafer containing nanoparticles diffused further into the brain tissue in comparison to the Gliadel wafer merely containing BCNU. Not only this, but the BCNU was also able to maintain at therapeutic levels for over 24 hours at the goal distance of 4cm from the tumor site.

The ability of BCNU to reach a distance of 4cm from the tumor site supports the success of our design. This result strongly suggests that this method of drug delivery may treat the malignant glioma more successfully when compared to alternative cancer treatments. Design recommendations to more accurately model this process include adjustments to the geometry, nanoparticle diffusion and degradation, and assumptions made within the cavity region.

## II. Introduction

A glioma is the most common type of brain cancer. It forms in the glial or supportive tissue in the brain and is a primary brain cancer, meaning that it develops from cells that originate within the brain. One such kind of glioma is an astryocytoma which forms from small star shaped cells called astrocytes. An astryocytoma can occur anywhere within the brain or even spinal cord. It occurs most often in adult cerebrum tissue. Astryocytomas are graded according to the severity of the tumor. A grade IV astryocytoma is called a glioblastoma multiforme and is categorized by aggressive growth and speed [22]. They account for more than 50% of all astryocytoma cases. Glioblastoma multiforme is also known to recur after surgical removal of the tumor within the 2-4cm radius past the edge of the original lesion [12].Symptoms of gliomas, which may slowly appear at first, include headaches, seizures, personality changes, weakness in arms or legs, and numbness. The intensity of symptoms may vary; and some patients may be diagnosed only after coming in for a totally different issue. The typical life expectancy is 6 to 24 months after initial diagnosis [23].

Surgery is the most common treatment method, with the biopsy being a key step in diagnosis. Surgery is used to remove as much of the tumor as possible, and the biopsied tissue is used to determine the tumor composition. The biopsy results determine which treatment is best [12]. There are two adjuvant treatments for tumors after surgery: radiation and chemotherapy. However, most cancerous glioma cells are partially resistant to chemotherapy and radiation [11]. Radiation therapy is used to treat high grade gliomas and recurrent gliomas. Two types of radiation therapy include stereotactic radiation (SRS) and brachytherapy. However, SRS is often not used due to an increased chance of radiation-induced toxicity. Brachytherapy's application is limited as well because it can only be applied to about 20% of brain tumors and can induce complications of homonymous quadrantanopia, focal necrosis, edema, and neurological disorientation [12]. Chemotherapy, including localized therapy, is sometimes used in combination with radiation after surgery. Currently, chemotherapy alone is the most common treatment.

One such chemotherapeutic method being used is the implantation of Gliadel wafer into the excised tumor cavity created post-surgery. Though a promising method, improving the diffusion of the release of drug can further improve this method. Gliadel wafers contain the drug Carmustine, or BCNU. BCNU is a cell cycle nonspecific akylating agent, affecting cells most when in their resting stage. BCNU attacks tissue by damaging the RNA and DNA responsible for proliferation which causes the cells to die or induce apoptosis because they can no longer divide. [5]

We will be working off the methodology from Gliadel to create an implantable localized treatment method that has BCNU incorporated into the wafer within spherical nanoparticles. The nanoparticles are present in the bulk of the wafer and are evenly dispersed. A polymer is being used in the hopes of protecting the drug from degradation as it diffuses, therefore allowing it to reach further into the tissue. The PSA nanoparticles will degrade via surface erosion. This will allow for a constant release of drug that is proportional to the amount of volume degraded of the

nanoparticle. By inserting these wafers directly into the tissue, they provide a sustained local chemotherapy at the site of the tumor. The total amount of BCNU within these nanoparticles will be equal to the total amount of BCNU within the Gliadel wafers to make a more accurate comparison of the methods. This is so that it better targets all the remaining cancerous, gliomal tissue with the toxic dose, while keeping a concentration low enough in the healthy tissues outside the 2-4 cm radius to protect them from apoptosis. For the current methods in use, BCNU does not reach this distance required to prevent recurrence. Reaching a 4cm distance into the tumorous tissue could potentially kill 98% of the remaining cancerous cells [10]. Making this possible during actually surgical operations could significantly reduce the mortality rate of this deadly disease.

## IIA. Design Objectives:

Using COMSOL, we will model the release of spherical nanoparticles from the wafer and the release of drug, BCNU, from the nanoparticles as they degrade with time. We will do this in order to:

1) Determine how BCNU diffuses through the brain from the wafer with time
2) Determine how far into the normal tissue BCNU is able to diffuse using this delivery method
3) Compare the nanoparticle delivery method with current delivery method used by Gliadel

## IIB. Problem Schematic:

In COMSOL, we used a 2D axisymmetric cylindrical model containing the tumor cavity where the tumor was removed, remaining tumor after surgery layer, wafer layer, and normal tissue domain. The cavity, tumor layer, and wafers were modeled as hemispheres with respective thicknesses of 14.5mm, 3.1 mm and 1mm. The normal tissue was modeled just beyond the tumor layer, covering a 10cm region. The nanoparticles were initially embedded within the wafers and encapsulate the drug, BCNU. The nanoparticles are made of PSA, known as poly(sebacic acid), whose molecules are linked together by anhydride bonds. These bonds split over time due to hydrolysis, which cause surface erosion to take place and BCNU to be released [12]. Both the diffusion of the nanoparticles from the wafers and the radial diffusion of BCNU from the nanoparticle were modeled. There is no BCNU present in any of the domains prior to release of the nanoparticles. BCNU modeled to be generated as a function of the concentration of BCNU per volume of nanoparticles, the concentration of nanoparticles, and the change in volume of the nanoparticles with respect to time. BCNU is released to diffuse and will degrade by first order kinetics. Further diffusion of BCNU into the normal tissue is anticipated due to its encapsulation within the nanoparticles, which protect the drug from degradation.

Convection was taken into account through the modeling of the interstitial fluid flow in each area of the brain based on the unique physical properties of the cavity, wafers, tumor layer,

and into the normal tissue. The fluid flow to the area is due to fluid being brought to the area by the vascular tissues. There is increased flow to the area following surgery as the body tries to heal itself, which causes pressure to build up in these vessels and fluid to leak out. Instead of modeling the complex vascular network present in the brain tissue, our model assumes a fluid generation term that models the increased fluid to the region. The schematic of the model is shown in Figure 1 below.

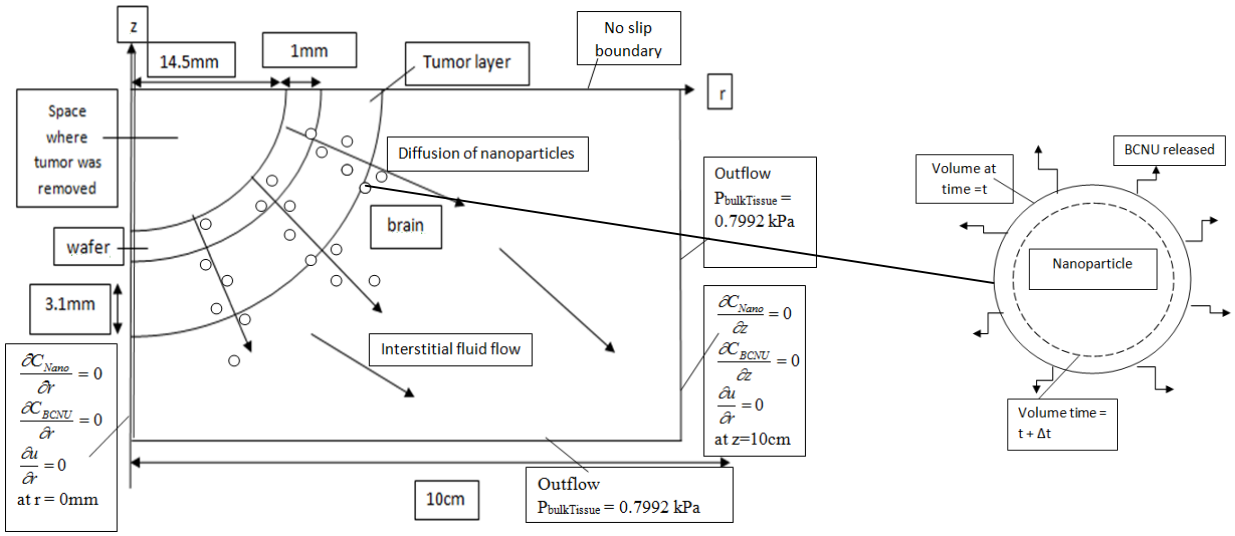


Figure 1: Schematic of 2D axisymmetric cylindrical model. The figure shows the cavity, wafer layer, tumor layer and normal tissue, as respectively labeled. The cavity is 14.5 mm radially, the wafers at 1.0 mm, and the remaining tumor layer left after surgery is 3.1mm. The rest of the domain extends to 100 mm and is considered to the normal brain tissue. The circles represent the nanoparticles outwardly diffusing from the wafers and the arrows next to the circles show the direction this diffusion. Further arrows describe the fluid flow, which is the same direction as diffusion. The boundaries of the domain are labeled with the boundary conditions used in the simulation. The right of the figure shows a zoomed in version of the nanoparticle. This close up shows a solid line around the edge of the nanoparticle showing the outline of the nanoparticle before volume was released and the dotted line shows the edge of the nanoparticle at a later time after surface erosion has taken place. The arrows pointing outward represent the BCNU release through surface erosion and the direction of diffusion.

Figure 1 shows the diffusion of nanoparticle from the wafer layer and through the tumor layer and into the normal tissue. Additionally, it displays the interstitial fluid flow in the brain as well as the boundary conditions applied to the overall 2D cylindrical model. The nanoparticles are shown more precisely on the right hand side of figure 1. The close up of the nanoparticle shows the release of BCNU from the nanoparticles, as well as how the volume of the nanoparticle decreases with time due to this release.

## III. Results

To determine how the BCNU moved throughout the tumor layer and into the normal tissue, our model was run for 12 days. Over this time period, the impacts on the concentration profile both during the edema at maximum value and as the edema decreased were observed.

Initially, the BCNU diffuses out the wafer symmetrically. There is a high concentration of BCNU closest to the wafer and a lower concentration of BCNU at an increased distance from the wafer layer. The symmetrical surface plot displaying the initial BCNU diffusion is represented by Figure 2 below.

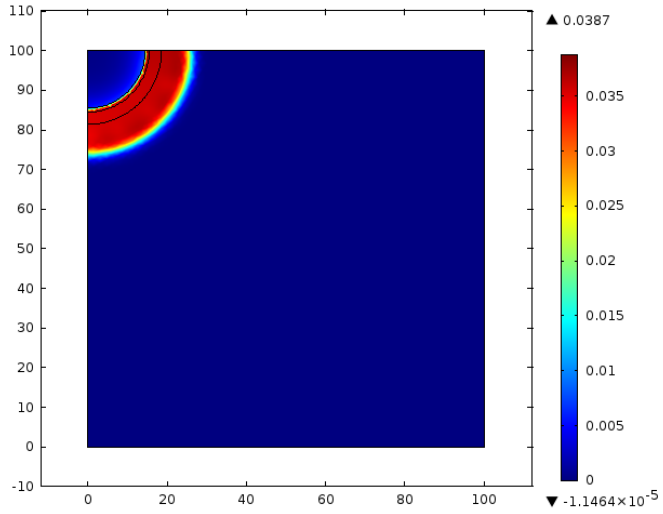


Figure 2: Surface Plot of Concentration of the Initial Diffusion of BCNU. The figure shows the concentration surface plot of BCNU at time = 16 hours. The colors on this plot represent different concentrations of BCNU in mg/mm$^3$ of tissue with the scale on the right of the figure. The red shows higher concentrations whereas the blue shows lower concentrations. The drug is only diffusing at this time point within the simulation because the edema is a maximum values, causing the only physics to be the simple diffusion of the drug. This creates a symmetrical drug diffusion pattern that is progressing radially away from the wafer layer in both directions.

This pattern of drug concentration modeled in Figure 2 occurs because the edema is at maximum values at this initial time period. Because the edema slows the velocity within the tissue, the nanoparticles and drug are only able to travel via simple diffusion, and therefore diffuse symmetrically. More about this is phenomenon is explained within the Edema section of the Sensitivity Analysis.

As the edema decreases and the excess fluid is released from the area, the pressure gradient reforms, and the bulk flow of fluid becomes significant again. This is shown in Figure 3 below which displays the concentration profile of our model after 12 days.

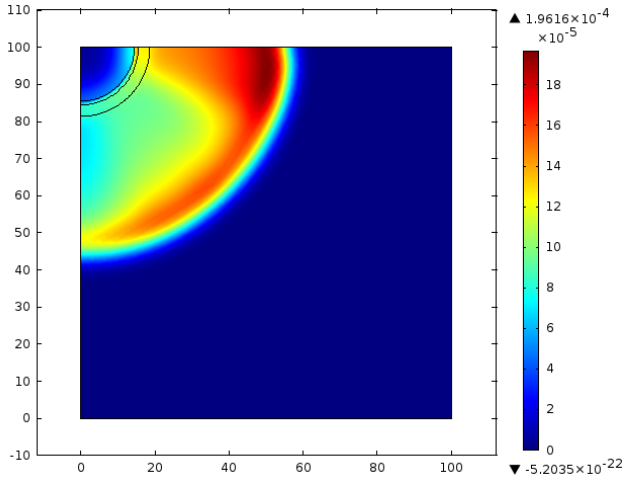


Figure 3: BCNU concentration profile at day 12. The concentrations of BCNU are not uniformly distributed radially and are greatest at the top of the normal tissue. The velocity is smallest at the top boundary because of an assumed no-slip condition. The velocity is also smallest further from the wafer because the pressure gradient is less significant at further radial distances. This causes a deposition of drug within the area closest to the top boundary and furthest from the wafer.

As seen in Figure 3, the decrease of the edema causes a shift from a symmetric to a non-symmetric diffusion pattern. This non-symmetrical nature of the drug is due to the no slip boundary condition assumed at the top of our geometry, which causes the fluid velocity to be slower in the areas surrounding this region. The velocity is also smaller the further from the wafer because the pressure gradient is less significant. Since the fluid velocity decreases, the drug is able to collect, and there will be higher concentrations present in this region compared to distances further away from the top boundary and/or closer to the wafer. Further distances from the top boundary have a greater continuous bulk flow and will thus have lower concentrations of drug.

Interestingly, even with the non-symmetrical concentration profile at the end of the simulation, the maximum penetration distance reached by the drug is the same at all radial points along the progressing drug front. The maximum penetration distance of the drug was considered to be the maximum distance from the edge of the removed tumor where the optimization function would reach zero at day 11. The characteristic curve seen at these distances is shown in Figure 32 in Appendix D. Figure 4 shows that the furthest radial distances from the wafer have very low values for velocity magnitude. This causes diffusion to be the main method of transfer for the BCNU at these distances.

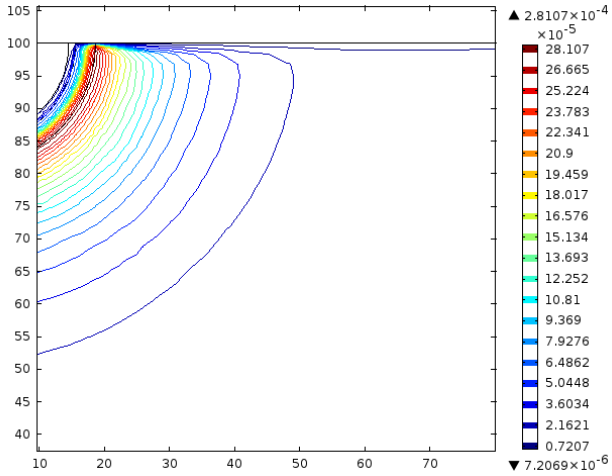


Figure 4: Contour Plot of Velocity in the Brain. The area closest to the top boundary has very low velocities due to the no slip boundary assumed there. The velocity contours are highest and most concentrated in the area by the wafer and tumorous tissue due to the high-pressure gradient presence there. The high-pressure gradient there causes more convective flow in that region. As distance increases radially from the wafer layer, the velocity decreases quite a bit, and isn't as significant as the velocities experienced closer to the wafers.

Because the drug front is already at a far enough distance as the edema decreases, the convective effects are not experienced by the front. Thus, diffusion of drug along the front continues symmetrically due to the lack of convective effects. The main pressure gradient, and hence velocity gradient, is formed in the area closest to the wafer layer, but as distance from the wafer increases, the velocity effects become less and less significant. This means that the penetration distance is symmetrical.

Therapeutic levels of BCNU reached to over the 4 cm point within the normal tissue. In order to be effective, the BCNU must be at the threshold value of $5.394 \times 10^{-12}$ mg/mm$^3$ of tissue

for at a minimum of 24 hours. Because Gliadel wafers produced therapeutic levels of BCNU for 24 hours at the distances reached, we were concerned with having our method create a drug presence for 24 hours. Even though the therapeutic drug concentration presence was only required to be 2 hours due to in vitro studies, we looked to have the therapeutic concentration of drug for 24 hours to make a better comparison to Gliadel's effect. The drug reached this desired concentration at our goal distance of 4cm from the edge of the removed tumor. This is shown in the Figure 5 below.

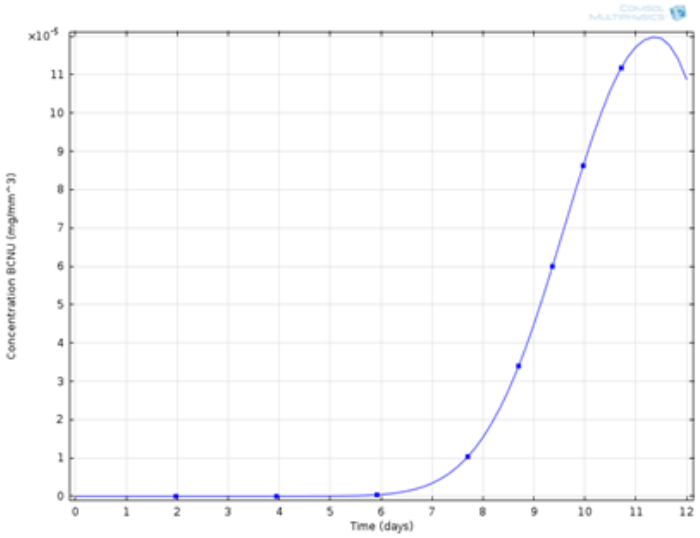


Figure 5: BCNU Concentration at 4cm from Removed Tumor. The concentration profile in the figure is taken at a distance of 4cm radially away from the edge of the tumor. The BCNU concentration reaches therapeutic values ($5.394 \times 10^{-12}$ mg/mm$^3$ of tissue) and rises well above it, with a maximum magnitude on the order of $10^{-5}$mg/mm$^3$ tissue. The concentration peaks around 11 days.

Figure 5 shows that the BCNU concentration reaches well above $5.394 \times 10^{-12}$ mg/mm$^3$ of tissue and remains at this concentration for well over 24 hours. Figure 6 below displays the optimization graph of the concentration of drug with increased distance from the cavity/tumor layer interface over 12 days. The optimization equation was considering the positive factor of having the drug at therapeutic levels, and negative factor of having the drug at toxic levels or below therapeutic levels. Concentrations below therapeutic levels occurred before the lines reached zero, and zero marked the point where the therapeutic value was reached. A spike following zero concentration would indicate toxic levels, or the drug degrading back to below therapeutic levels.

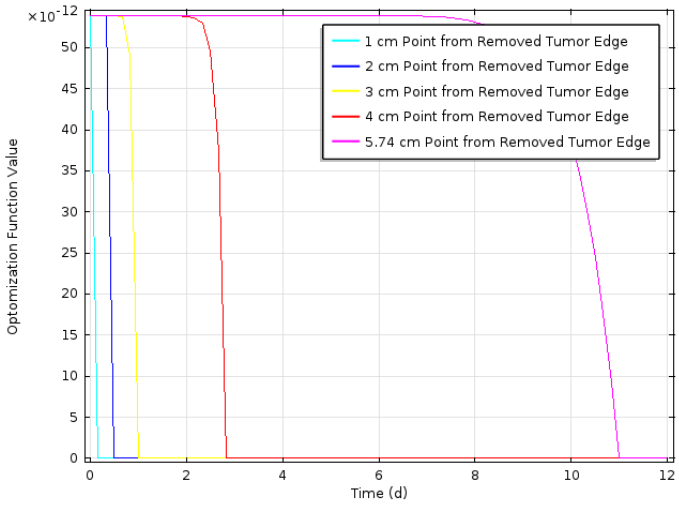


Figure 6: Optimization Function for the Concentration of BCNU into Normal Tissue for 12 days at various distances. The optimization function used assigned positive values equal to the difference between the current concentration and therapeutic levels. If a concentration was at or above therapeutic levels while below toxic levels, the optimization function assigns that point a value of zero. The drug reaches therapeutic levels of BCNU at around day 3 at the 4 cm goal point. The drug is able to reach an ultimate penetration distance of 5.74 cm from the edge of the removed tumor. This is well above the distance reached by the current Gliadel method.

In Figure 6 it can be seen that at a distance of 4cm from the edge of the removed tumor, the optimization value reached zero, indicating that therapeutic concentrations were reached at this distance, around day 3. The drug remained at therapeutic levels for all distances less than 4 cm for majority of the 12 days of the simulation. As stated above, the maximum penetration distance of the drug was considered to be the maximum distance from the edge of the removed tumor where the optimization function would reach zero at day 11. This would mean that the drug was at therapeutic levels for a day of our simulation, which was comparable to the current method of treatment that has therapeutic levels of BCNU for approximately a day. The maximum distance reached in this model was 5.74 cm. The true penetration distance may be even further than that, but our simulation is limited by the time it was run. If the model were run longer, the true penetration distance would be the maximum distance from the edge of the tumor where therapeutic concentrations of BCNU were reached for a minimum of one day. Because the simulation was only run for 12 days, there may be a distance where therapeutic levels of BCNU were reached at a day past day 12 and were present above that level for a day.

As mentioned above, Gliadel wafers are the current method of treatment. Clinical trials have shown that therapeutic levels of BCNU are reached at a limited distance from the wafer. Most papers cite a penetration distance of a mere 1-2cm from the edge of the resurrected tumor, and the drug is only present at this distance for approximately 24 hours. This indicates that this treatment method needs to be improved. Our model has shown the ability to achieve the distances reached by the current delivery method and far succeed them. Encapsulating the BCNU within nanoparticles, allows for the drug to therapeutically treat the cells up to 5.74 cm from the edge of the tumor resection cavity, and can therefore efficiently treat a much larger region than the current Gliadel wafers are able. It also provides the cells with a more consistent, continuous exposure the to BCNU which can make the anti-proliferative effects of the drug more efficient to the larger range of penetration. This larger treatment zone can lead to less recurrence of tumors and hence and increased survival rate for those diagnosed with MGB.

## IV. Mesh Convergence

An analysis of our model's simulation mesh was done to ensure that our results were as accurate as possible to prevent discretization errors. We were aiming to have our results maintain certain accuracy while not having COMSOL perform unnecessary calculations. The concentration of BCNU 2 cm from the wafer within the normal tissues was analyzed at times of 800,000 and 900,000 seconds. The mesh spanning the tumor region and the wafer region was necessitated to be extremely fine because the highest rates of change occur within these regions. Hence, only the numbers of elements in the portion of the mesh outside of the wafer and tumor region, and within the cavity and normal tissue domains, were changed. The mesh was analyzed for convergence by changing these portions of the mesh to various predefined meshes.

When changing the mesh to a size of less than 7702 elements, a computing error would occur because the mesh would not converge. This was due to the fact that there were not enough elements to accurately give a solution to the problem. A custom maximum element sized mesh was then used in conjunction with the remaining regions set to the finest predefined mesh possible. The maximum element size was slightly decreased in order to further analyze how many elements were needed for an accurate solution. The total number of elements was then plotted against the concentration of BCNU at specific times equal to 9.26 and 10.42 days at the defined point 2 cm from the wafer within the healthy tissue called '2cm into normal tissue'. This was used because it was not within the tumor or wafer region whose mesh was already defined and was not as far out as our goal point, which may have had many times were the concentration was zero. This made analyzing any change in concentration, at this point at a specific time, due solely to the change of mesh size easier. The graphs where the concentration values were taken at 9.26 and 10.42 days are shown below in Figure 7.

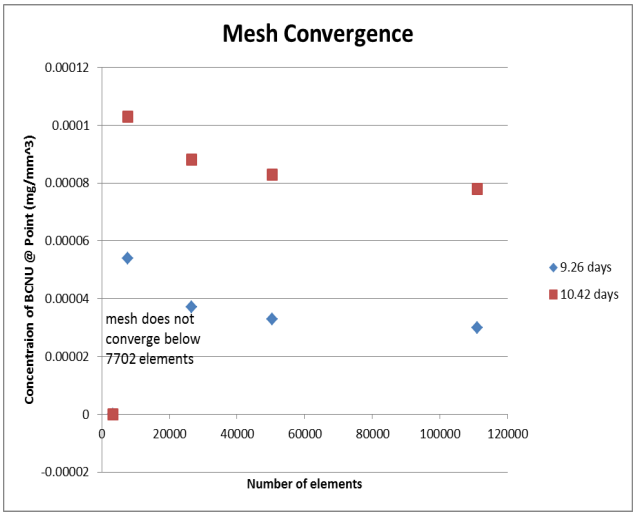


Figure 7: Mesh Convergence of BCNU Concentration at 2 cm into the normal tissue at times 9.26 and 10.42 days verses the number of elements. The mesh appears to converge at 7702 elements due to the concentration varying very little with a very large increase in element number.

The mesh converges and no more significant change in accuracy of the solutions is seen after a mesh of 7702 elements, as shown. In Figure 8, it is shown from the plateau in values that

a mesh of 7702 elements is sufficient enough and that more elements than this will not significantly increase the accuracy of the solution.

Figure 8 below shows the final mesh chosen. The difference in element size between the tumor/ wafer region and the remaining tissue is shown by the differences in the element size and the density of the elements.

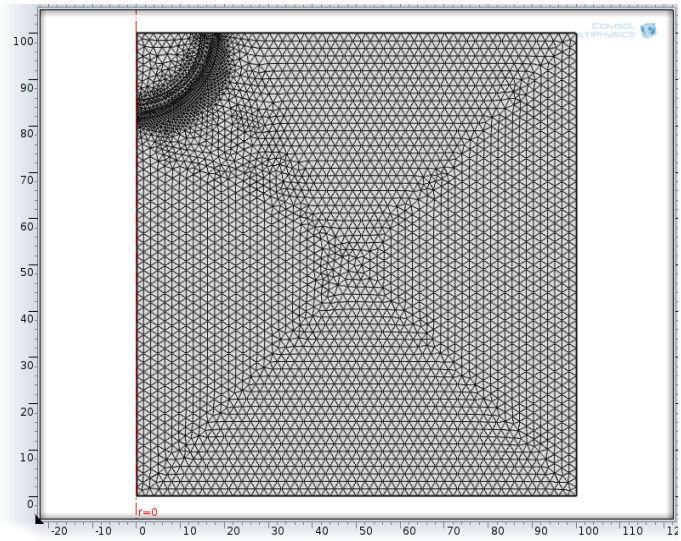


Figure 8: Final mesh for the model. This mesh consists of 7702 elements, which is the number of elements at which the solution converged. There is a much higher density of elements in the region of the tumor and wafer layers due to this being the region with the highest amount of change. A finer mesh was used within the cavity and outlying normal tissue regions.

As shown in Figure 8, the difference in element size between the tumor/ wafer region and the remaining tissue is evident. It is also clear that the values and shape of the BCNU concentration graph at 2cm into the normal tissue does not significantly change at a mesh finer than 7702 elements. Though meshes with a larger number of elements give slightly more accurate answers, the concentration solution value differences are to the power of $10^{-5}$, meaning the differences between each mesh's solution is small enough that the extra calculation time in COMSOL would be quite significant in relation to the small amount of added accuracy. Table 1 in Appendix D shows each trial that was run, under each number of elements, and the solutions that were produced.

## V. Accuracy Check

### i. Pressure

Our model included the added complexity of accounting for the interstitial fluid flow within the brain that aids in the transport of drug. We made simplifications of the true process and so compared the fluid specific properties of our model to other experimental and simulated values. Figure 9 below shows the pressures associated with each region of the brain within our domain.

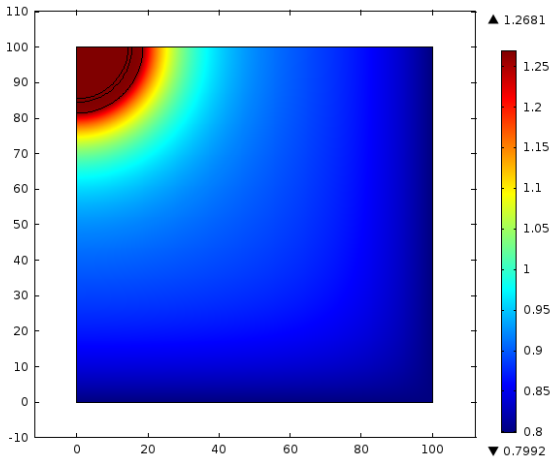


Figure 9: Surface Plot of Pressure in the Brain Excluding the Impacts of the Edema. The pressure in the cavity and wafer layer are the highest (red), followed by the tumor layer (lighter red), and last the model tissue (yellow to blue). This shows a pressure gradient (high to low) from the cavity to the normal tissue.

Figure 9 shows that the pressure is highest in the cavity, then in the tumor layer, and last in the normal tissue. This pressure gradient accounts for the velocity and direction of fluid flow within the brain.

### a) Pressure in Cavity

Figure 25 in Appendix D displays the pressure of our model over a period of 3 days. During the first 3 hours our model stayed at the constant pressure of approximately 1,280 Pa. In comparison, Figure 24 in Appendix D shows the pressure values from literature increasing in steps over the 3 hour period before reaching the steady-state pressure of 1000 Pa just after 2 hours. This increase in pressure is due to the pressure associated with the cavity filling up with interstitial fluid. Because our model assumed that the cavity was already full, there was no increase in pressure, but instead began at the steady state condition. This was an acceptable assumption because our 12 day model had a time step of 4 hours, and due to the limits of computing time and power, the variance seen in the 3 hours of the literature model would not be visible in our model. The steady state values of our model and the literature model are consistent, thus verifying our assumption.

### b) Pressure in Tumor Layer

Figure 27, in Appendix D, shows our model of pressures throughout the tumor layer in the first 3 hours is the same as that in the cavity and shows a steady line at 1,280 Pa. In comparison, in Figure 26, in Appendix D, the pressure values from literature show a sharp decrease from 1,200 Pa to 500 Pa before 0.5 hours. This decrease is due to the vast decrease in pressure as fluid flows into the cavity. At this point there is a large pressure difference between the cavity and the tumor layer as the interstitial fluid is driven into the cavity from the tumor layer. Pressure is driven to a minimum value at this point and then recovers and again rises in steps until a steady-state value of 1000 Pa is reached just after 2 hours. Again, because our model assumed that the cavity was already full, there was no decrease in pressure, but instead

began at the steady state condition of pressure. The steady state values of our model and the literature model are consistent, thus verifying our assumption.

#### c) Pressure in Normal Tissue

Figure 29, in Appendix D, shows our model at a steady pressure at 915 Pa in the normal tissue during the first 3 hours. In comparison, in Figure 28 (Appendix D) the pressure values from literature encounter a decrease from 900 Pa to 700 Pa before 0.5 hours and then rise in steps until they reach a value of 900 Pa. This is similar to that of the tumor layer in that pressure drops within the first 30 minutes as the cavity fills and then rises until it reaches steady-state. In the normal tissue, our pressure values are the same at steady-state as those pressure values in the literature.

#### d) Pressure Conclusions

As explained in the above sections, our pressure values are comparable with those found in other simulations in literature. Because of this, the error due to the simplification of having the cavity full and pressures at steady state initially is limited.

### ii. Velocity

Figure 10 below shows the interstitial fluid flow within the brain. The arrows show the direction of the velocity but are not to scale of the magnitude of the velocity at each point.

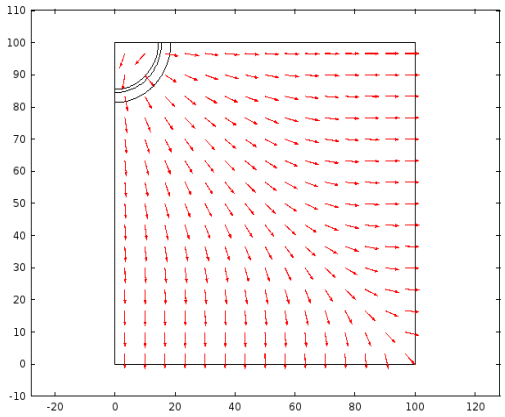


Figure 10: Arrows Showing Velocity Direction in the Brain. The high pressure in the cavity and the lower pressure present in the normal tissue creates a pressure gradient. This pressure gradient causes a direction of flow down the pressure concentration gradient. This is seen in the figure by the arrows point in the direction from the wafer boundary to the outflow boundaries on the right and bottom edges of the model geometry.

The figure above shows that the fluid flows out from the cavity region, through the tumor layer, and into the normal tissue. The surface plot of pressure and the velocity arrow plot is overlaid and shown in Figure 10.

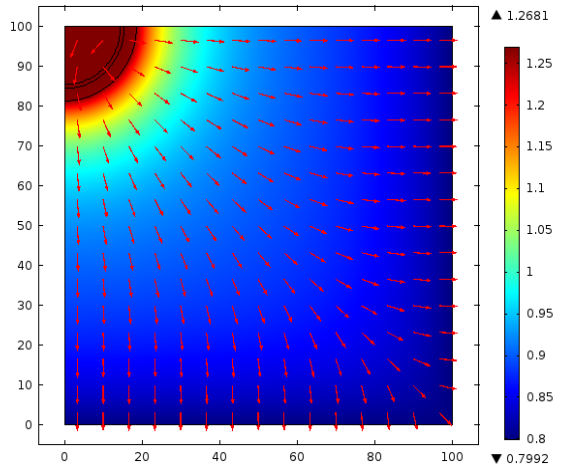


Figure 11: Velocity Direction Overlaid on Pressure Surface Plot in the Brain. It is more clear in the figure that the velocity directionality is consistent with the direction of the pressure gradient. The pressure is highest in the cavity, and lowest on the boundary of the normal tissue, causing the fluid to flow outward and away from the wafer layer.

Figure 11 shows that the direction of the fluid flow is due to the pressure gradient. Because the pressure is significantly higher in the cavity region than in the tumor layer and normal tissue, the fluid flows outward from the cavity and into these regions.

The average interstitial fluid velocity in the brain is $6.5 \times 10^{-6}$ mm/s. As displayed by the pressure surface plot, shown in Figure 9, the pressure gradient in the tumor layer is significantly higher than that of the normal tissue and cavity. This is because there is such a great difference in pressures from the cavity to the tumor layer and through the tumor layer into the normal tissue. Additionally, distances further and further into the normal tissue are farther from the high pressures associated with the cavity region and therefore farther from the concentration gradient. As a result, the pressure in the normal tissue is lower than that of the tumor layer. Because of this, the fluid flows at a higher velocity in the tumor layer, at a value of $4.6 \times 10^{-4}$ mm/s. Our results also show that the tumor layer has a higher velocity in comparison to both the normal tissue and the cavity, with a magnitude difference of 10. This can be seen in Figures 30 and 31 in Appendix D. Figure 30 shows that the velocity in both the cavity and the normal tissue has an approximate magnitude of $10^{-6}$ mm/s. This is comparable to the value of $6.5 \times 10^{-6}$ mm/s found in literature. Figure 31 displays the velocity of the tumor layer and it is shown to be in the order of magnitude of $10^{-5}$mm/s. This shows that the pressure in the tumor layer is lower than that of the cavity and normal tissue as described in literature and in relation to the surface plot pressure gradient. The correlation of the values found in literature to the values found within our model verifies our model as accurate with respect to velocity magnitude.

### iii. Concentration

Many clinical trials and experiments have been done to study the penetration of BCNU into brain tissue after an implant with the commercially available Gliadel wafers. We altered our model to exclude the nanoparticles in order to show how our model's parameters compare with the in vivo studies done. Experiments done on rat brains showed that the main transport of drug was due to convection and diffusion alone, however when the experiments were done on non-human primates a different phenomenon was observed. In the paper by Fleming and Saltzman [9], it was explained that the non-human primate studies revealed another transport mechanism in addition to convection and diffusion that was not observed in smaller species. These studies noted the presence of BCNU within 1-2cm from the edge of the wafers, on the order of $10^{-14}$-$10^{-13}$mg/mm$^3$ of tissue for up to 7 days after the implantation. This result was also observed in the studies done by Fung, Ewend, Sills, et al. [26] where significant concentrations of BCNU were observed at that distance after a period of time after implantation. It was hypothesized that the other transport mechanism involves BCNU being transferred into cerebrospinal fluid or the blood stream and then redepositing into the brain tissue.

In Fleming and Saltzman's simulated human brain model, they noticed a peak of BCNU around 6 hours, and then a short but sharp decline that was followed by a slower decline over the next few days. Our model showed a similar trend with significant BCNU levels present within 1.75 cm region past the wafer layer as shown in Figure 13 below.

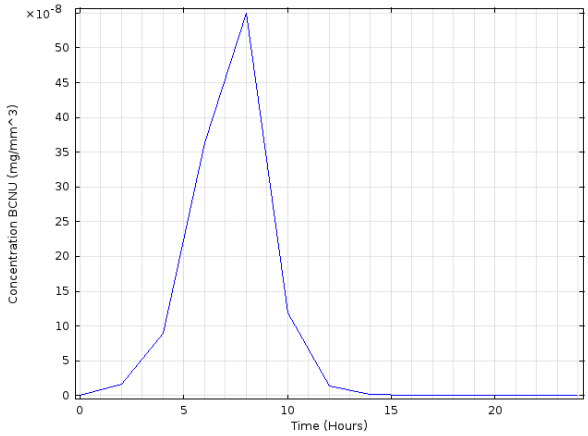


Figure 12: Concentration of BCNU 1.75cm from the Cavity/Tumor Interface. There is a sharp peak of BCNU concentration around 8 hours. This is followed by a sharp decline in concentration for the subsequent hours. The plot appears to reach zero at time=15 hours, but in fact it reaches zero at hour 20. It appears to be zero at hour 15 because of the large scale difference between the values for concentration that occur at early times vs later times. The later times have concentrations that are quite a few orders of magnitude different than early times, so the actual value are so small in comparison that they appear to be zero.

According to Figure 12, the BCNU concentration peaks at around 8 hours, and then has a sharp decline in the hours after peaking, followed by a slowed decrease. This is all consistent with Fleming and Saltzman's simulation. The scale on the Figure 12 above does not allow for one to see the presence of BCNU at much lower concentrations such as those seen in the mentioned studies. Figure 13 below, shows the graph above for the time 16-24 hours.

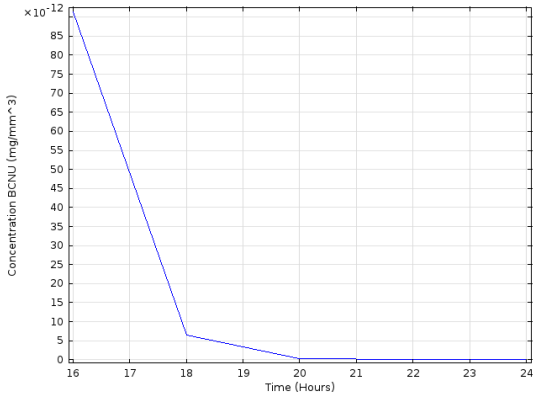


Figure 13: BCNU Concentration 1.75cm From the Cavity/Tumor Interface. This figure shows that at times after 15 hours the concentration is not yet zero despite appearing as such in Figure 12. The magnitude of the values is much smaller at these times than the magnitude of the values at earlier times, making it difficult to see the presence of concentration after hour 15.

As Figure 13 shows, the concentration of BCNU is not yet zero, and is still at therapeutic levels at this time at 1.75 cm past the wafer in the tissue. Around hour 21 the concentration is so much lower at this point than in other points of the domain that COMSOL has trouble handling it. It starts to produce inaccurate values of concentration thus it is unclear the concentrations after this point.

Our model seems to follow the other clinical data, as well as other simulations, of the process for the first day, but after the first day the models diverge. The first rate kinetics of our simulation cause the degradation of BCNU, which is a very high rate due to the drug's half life of 31.2 minutes, to eliminate any drug left in the domain by the end of 1 day within the model. If BCNU was taken up by the CSF or blood stream and then were to reenter the tissues, this would not be visible in our simulation, and could be the reason for the discrepancy between the in vivo studies and our model. This gives confidence to our model with the inclusion of nanoparticles, on the note that the BCNU will potentially be able to linger in the tissue regions surrounding the implant for even longer than shown in this simulation. This means that a therapeutic dose will be available in the tissues for longer times than expected, which may lead to a higher effectiveness in the use of nanoparticles.

## VI. Sensitivity Analysis

### i. Edema Length

After the surgery to remove the main tumorous portion of the brain, an edema is likely to be produced within the brain tissue surrounding the cavity. The edema was modeled by having the permeability of the vascular network increased to be 100 times the baseline value during the time of full edema. The increased permeability causes increased fluid volume within the normal tissue and the remaining tumor tissue, thus causing the pressure in the tissues to reach a constant value across the domain. This then causes the pressure gradient that had formed between the cavity and normal tissues to disappear. Without the pressure gradient, the flow within the tissues

slows quite significantly. This slowing of fluid causes the nanoparticles and drug to move only via diffusion, and hence would not be able to move as far as if the pressure gradient had been maintained. The longer the edema is at maximum values, the longer the fluid will be at slowed rates. The longer the fluid is at slowed rates, the less the BCNU is able to travel by convection. The less the BCNU is able to travel by convection, the less the BCNU will be able to penetrate the tissue.

Edema time is considered to be the time spent at maximum values for hydraulic conductivity. The drug is able to reach therapeutic levels for the edema times of 12 hours, 24 hours, 3 days, and 7 days. This was determined by finding the point past the wafer at which the optimization plot reached zero at the time t=11 days. The plot shown in Figure 16 below shows the curve that the maximum distance of penetration produced for each edema time.

Since edema length varies from person to person and surgery-to-surgery, it is difficult to approximate a person's edema length to know if the therapeutic levels will be reached at the 4cm distance. The effects caused by the edema during in vivo monkey studies seemed to be resolved after 3 days, indicating that the edema was present at maximum values for 1 day, which why that value of edema time was used in our model [9]. Figures 14 A and 14 B below show how the maximum therapeutic distance reached by the drug was changed for each varying edema time.

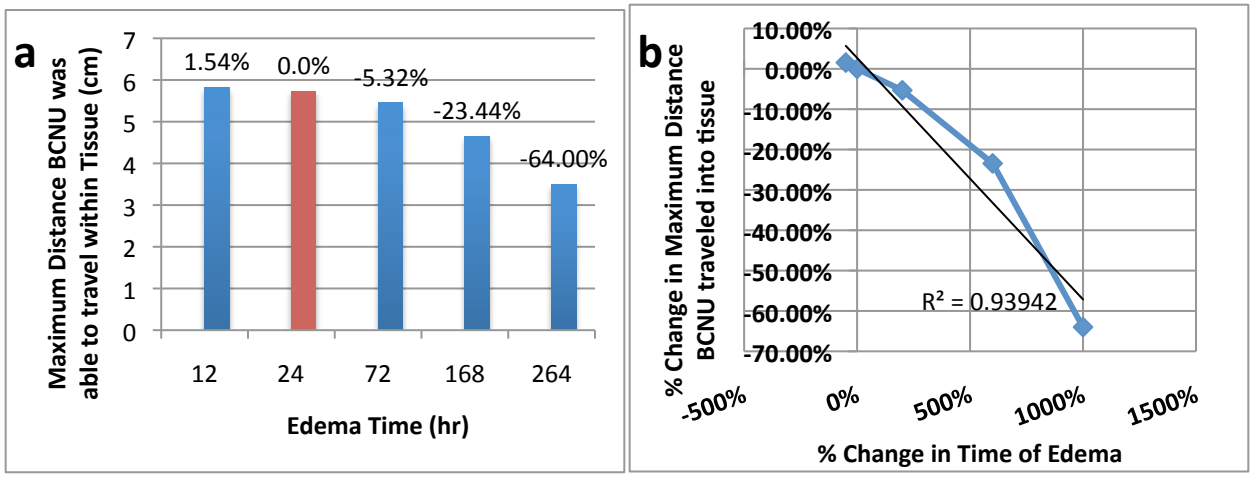


Figure 14: (a) Edema Time vs. Distance. As expected, as the edema time decreases, there is an increase in penetration due to the fact that the velocity within the tissue is decreased for a shorter period of time. As the edema time increases, there is a decrease in penetration distance. For he edema time of 264 hours or 11 days, the drug doesn't reach the maximum goal distance of 4 cm and only is able to reach a distance of approximately 3.5 cm. (b) Figure 15: %Change in Edema vs. Distance. The percent change in penetration distance of the drug has a decently linear relationship with the percent change in edema time. The $R^2$ value is approximately 0.94, which indicates a good sense of linearity. This $R^2$ value could be improved by testing more edema times and plotting more values for the change in penetration distance.

As seen in Figure 14a above, as the edema time increases, the maximum therapeutic penetration distance decreases. Figure 14b shows that the percent difference in distance varies semi-linearly with the percent change in edema time showing an inverse relationship between the variables. This could help when predicting how far the drug has reached in a patient, after the edema time is known. The maximum distance is still above our target for times 7 days and

lower, which is promising news due to the fact that edemas often don't last past a week's time. This means that majority of patients will receive a therapeutic dose at 4cm.

### ii. Initial Concentration of Nanoparticles in the Wafers

Based on the size of the wafer, an approximation was made as to the amount of nanoparticles that could be embedded inside of the wafer. As shown in the calculations in Appendix B, there is a range for the radius of the nanoparticle and therefore a maximum amount of nanoparticles that could be fit into the wafer. Since the diameter of the nanoparticle is 186 ± 25 nm, when using the lower limit of 161 nm, the approximate number of nanoparticles that could fit in all eight wafers is $192 \times 10^6$. When this number is divided by the total volume of all eight wafers, the maximum concentration of nanoparticles is 145340 nano/($mm^3$ wafer). The same process was applied to the rest of the range of total nanoparticles and the differences in the distance of BCNU that traveled into the normal tissue at therapeutic levels is shown in Figure 15a (See Appendix B for range).

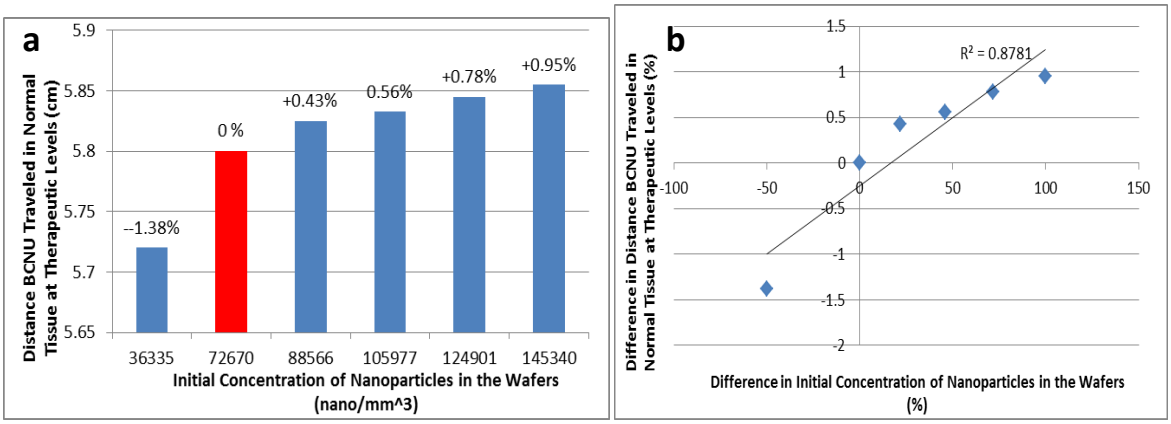


Figure 15: (a) Concentration of Nanoparticles vs. Distance. As expected, there was a decrease in the distance traveled, when there was a decrease in nanoparticles concentration in the wafers, and an increase in distanced traveled with an increase in concentration of nanoparticles in the wafer. The bar in red represents the original value that was tested. When the maximum concentration of nanoparticles in the wafers was tested, there was a small increase and when the minimum concentration of nanoparticles in the wafers was tested, there was a small decrease. Therefore, this was not a very significant value to estimate, and our value did not have a great impact on our results. (b) Percent Change in Concentration of Nanoparticles vs. Percent Change in Distance. The percent change in penetration distance of the drug has a slightly linear relationship with the percent change in concentration nanoparticles in the wafers. The $R^2$ value is approximately 0.8781, which shows there some correlation with the data points. This $R^2$ value could be more realistic with more changes in the parameter value tested.

As seen in Figure 15a, by increasing the initial concentration by 100%, there was only an increase in the distance traveled by 0.95%. Also, when the initial concentration was decreased by 50%, there was only a decrease in the distance traveled by 1.38%. Therefore, the initial concentration of nanoparticles in the wafer does not have a significant effect on the model, and the ability of the nanoparticles to deliver BCNU to the brain. Figure 15b shows that the distance BCNU traveled does not show a direct correlation to initial concentration of nanoparticles in the wafers. Therefore, more values for this parameter should be tested to get a better relationship of changes in initial concentration of nanoparticles in the wafer, with difference in distance BCNU traveled in the normal tissue at therapeutic levels.

### iii. Initial Concentration of BCNU within each Nanoparticle

When changing the radius, another parameter that will be changed would be the initial concentration of BCNU within each nanoparticle. Therefore, using the range of total nanoparticles, which was used in the sensitivity analysis for initial concentration of nanoparticles, the initial concentration of BCNU was calculated (see Appendix B).

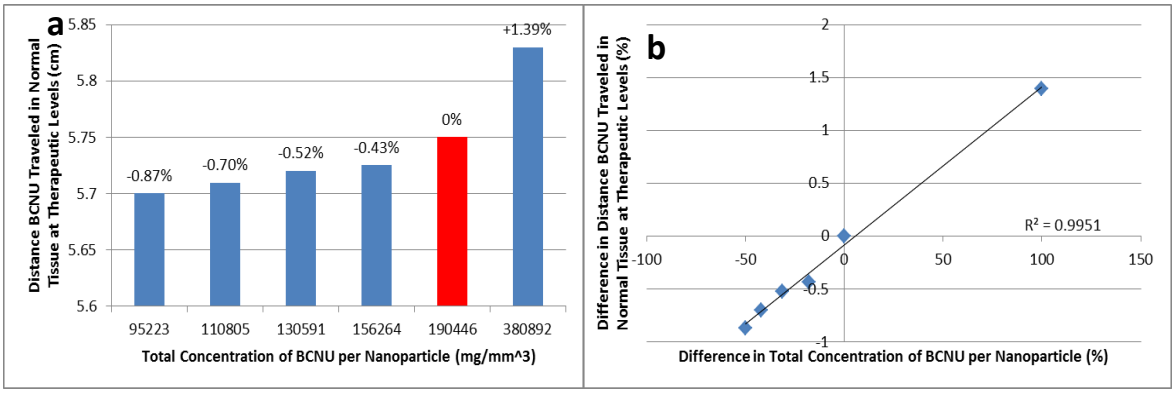


Figure 16: (a) BCNU vs. Distance. When changing the total concentration, of BCNU per nanoparticle, an increase in this value caused an increase in distance traveled, and a decrease in this value caused a decrease in distance traveled. The bar in red represents the value used in the original model. When the maximum BCNU concentration per nanoparticle was tested, there was a small increase and when the minimum BCNU concentration per nanoparticle was tested, there was a small decrease. This parameter estimation did not significantly impact our model. (b) Percent BCNU vs. Distance. The percent change in penetration distance of the drug has an almost perfect linear relationship with the percent change in concentration of BCNU per nanoparticle. The $R^2$ value is approximately 0.9951, which shows there is a linear correlation with the data points. This $R^2$ value could be more realistic if more values were tested.

As shown in Figures 16a, when the maximum concentration of BCNU per nanoparticle was used, which was 100% more than the original value there was only an increase of 1.39%. When there was a decrease in concentration of BCNU per nanoparticle by 50% there was only a decrease in distance traveled by 0.87%. Therefore, this parameter does not have a significant effect on the model, and the ability of the nanoparticles to deliver BCNU to the brain. Figure 16b shows that the distance BCNU traveled can be roughly estimated, based on change in the total concentration of BCNU per nanoparticle.

### iv. Diffusivity of Nanoparticles

The diffusivity of the nanoparticle is based off of the Einstein-Stokes equation as seen in Appendix C. However, for this equation, the brain matter was modeled under the assumption that the tissue is a viscous fluid. There could be factors that cause this assumption to be incorrect.

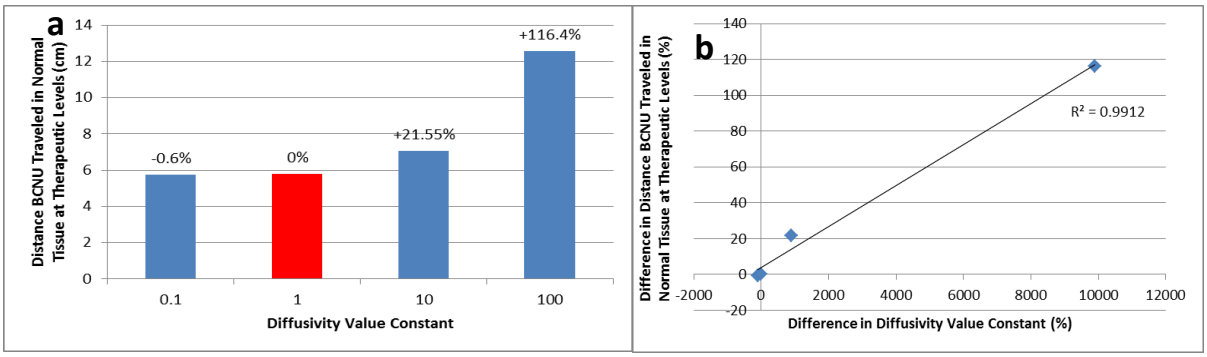


Figure 17: (a) Diffusivity vs. Distance. When the diffusivity was decreased by a factor of 10, there was a very small decrease in the distance traveled in the normal tissue at therapeutic levels. The red bar indicates the diffusivity used in our model and is multiplied by a constant of 1, so there is no change in diffusivity. When the diffusivity was increased by a factor of 10 and 100, there is an increase of distance traveled by 21.55% and 116.4% respectively. These values, show that when increasing the diffusivity by factors of 10 show a significant change in results. (b) Percent Diffusivity vs. Percent Distance. The percent change in penetration distance of the drug has an almost perfect linear relationship with the percent change in diffusivity. The $R^2$ value is approximately 0.9912, which indicates a good sense of linearity. This $R^2$ value could be more realistic if more diffusivity constant values were tested.

As shown in Figures 17a, when the diffusivity of the nanoparticle was decreased by a factor of 10, the distance that the BCNU traveled at therapeutic levels only decreased by 0.6%. When the diffusivity was increased by a factor of 10 and 100, there was a very steep increase in the distance traveled. However, there is no physical reason why the diffusivity would actually increase, and so there is no real significant effect when testing realistic diffusivity values. The linearity of the percent change in diffusivity versus percent changed in distance traveled can show how different polymers with known properties can travel in the brain (Figure 17b).

## VII. Conclusions

In comparison to the commercially available Gliadel wafers, our delivery method using nanoparticles was more efficient. BCNU was present in the tissue at a further distance from the cavity edge for longer periods of time. The BCNU was present in the tissues past our drug goal point of 4cm, and even reached to 5.8cm at the appropriate therapeutic concentration for the required time period of 2 hours. BCNU would be able to reach the appropriate distances and would be present in the tissue for longer which may lead to increased efficacy of the drug being able to treat all the cells in the region rather than just a fraction. We conclude that our drug delivery method would be more efficient than the current method used and would be able to prevent recurrence of tumor formation.

## VIII. Design Recommendations

To enable this model to more realistically portray the modeling of nanoparticle infused wafers within the brain, a few additional factors could be included in the model. One design recommendation would be to more accurately model the geometry. This could be done by modeling the brain in 3D. This would account for diffusion and convection in all 3 dimensions and offer more accurate results. Additionally, individual wafers could be modeled as opposed to

the wafer layer as a whole. This is because the wafer layer doesn't always form a perfect spherical shape and sometimes resembles more of a polygon. Modeling individual wafers would take care of any problems with the geometry of the wafers when described as a whole as well as make fluid flow more accurate. This is because interstitial fluid flow through and around the wafers could be more precisely defined when looking at the individual geometry.

Next, a design recommendation for the nanoparticles would be the inclusion of diffusion through the nanoparticles as well as surface erosion. Our model currently only shows the surface erosion associated with the nanoparticles and the diffusion through them could impact our model. Additionally, a moving mesh could model the surface erosion of the nanoparticles more accurately in comparison to the equations that we used and consistent mesh. The model could also be run for the full time period that the BCNU diffuses through the brain (3 weeks). This would provide more information on how the BCNU varies with time.

Last, another improvement would be to include convection in the cavity (space where the tumor was removed). Once the tumor is removed, the cavity is initially filled up with fluid due to the interstitial fluid flow. Once this reaches steady-state, the convection flow follows a more simplified flow pattern. Our model assumed that the cavity was already at steady-state in order to simplify it. This is not realistic and convection in the tumor cavity should be included for accuracy.

# IX. Appendix A: Model Design

## Governing equations:

### i. For Diffusion of Nanoparticles:

$$\frac{\partial C_{Nano}}{\partial t}+\left(v_r\frac{\partial C_{Nano}}{\partial r}+v_z\frac{\partial C_{Nano}}{\partial z}\right)=D_{Nano}\left(\frac{1}{r}\frac{\partial}{\partial r}\left(r\frac{\partial C_{Nano}}{\partial r}\right)+\frac{\partial^2 C_{Nano}}{\partial z^2}\right)$$

### ii. For Diffusion of BCNU:

$$\frac{\partial C_{BCNU}}{\partial t}+\left(v_r\frac{\partial C_{BCNU}}{\partial r}+v_z\frac{\partial C_{BCNU}}{\partial z}\right)=D_{BCNU}\left(\frac{1}{r}\frac{\partial}{\partial r}\left(r\frac{\partial C_{BCNU}}{\partial r}\right)+\frac{\partial^2 C_{BCNU}}{\partial z^2}\right)+R_{BCNU}$$

$$R_{BCNU}=BCNU_{Gen}-k_{BCNU}C_{BCNU}$$

$$BCNU_{Gen}=\left(1.90446\times10^5\frac{mgBCNU}{mm^3Nano}\right)(NanoPartDeg)C_{Nano}$$

### iii. For Convection using Brinkman Equation:

$$\frac{\rho}{\varepsilon_p}\frac{\partial u}{\partial t}=\nabla\bullet\left[-\rho I+\frac{\mu}{\varepsilon_p}\left(\nabla u+(\nabla u)^T\right)-\frac{2\mu}{3\varepsilon_p}(\nabla\bullet u)I\right]-\left(\frac{\mu}{K_{br}}+\beta_F|u|+Q_{br}\right)u+F$$

$$Q_{br}=\rho(\nabla\bullet u)$$

## Boundary Conditions:

### i. For Diffusion of Nanoparticles:

$\frac{\partial C_{Nano}}{\partial r}=0$ at r = 0mm, due to symmetry

$\frac{\partial C_{Nano}}{\partial z}=0$ at z = 100 mm

Outflow allowed at z = 0 mm and at r = 100 mm

### ii. For Diffusion of BCNU:

$\frac{\partial C_{BCNU}}{\partial r}=0$ at r = 0mm, due to symmetry

$\frac{\partial C_{BCNU}}{\partial z}=0$ at z = 100 mm

Outflow allowed at z = 0 mm and at r = 100 mm

### iii. For Convection:

$\frac{\partial u}{\partial r}=0$ at r = 0mm, due to symmetry

$\frac{\partial u}{\partial z} = 0$ at z = 100 mm, no slip condition

Outflow allowed at z = 0 mm and at r = 100 mm

$P_{bulkTissue}$ = 0.7992 kPa at z = 0 mm and at r = 100 mm

## Initial Conditions:

### i. For Diffusion of Nanoparticles:

$C_{Nano,\ Cavity}$ = 0 nano/mm$^3$ of cavity

$C_{Nano,\ Wafer}$ = 7.267 x 10$^4$ nano/mm$^3$ of wafer

$C_{Nano,\ TumorTissue}$ = 0 nano/mm$^3$ of tissue

$C_{Nano,\ NormalTissue}$ = 0 nano/mm$^3$ of tissue

### ii. For Diffusion of BCNU:

$C_{BCNU,\ Cavity}$ = 0 mg/mm$^3$ of cavity

$C_{BCNU,\ Wafer}$ = 0 mg/mm$^3$ of wafer

$C_{BCNU,\ TumorTissue}$ = 0 mg/mm$^3$ of tissue

$C_{BCNU,\ NormalTissue}$ = 0 mg/mm$^3$ of tissue

$C_{BCNU,\ Nano}$ = 0 mg/mm$^3$ nano

### iii. For Convection:

$P_{TumorTissue}$ = 1.2 kPa

$P_{NormalTissue}$ = 0.9 kPa

$V_{Cavity}$ = 0 mm/s

$V_{Wafer}$ = 0 mm/s

$V_{TumorTissue}$ = 0 mm/s

$V_{NormalTissue}$ = 0 mm/s

## X. Appendix B: Calculations

**Nanopartile Degradation Term:**

$$NanoPartDeg = \frac{dVol}{dt}\frac{mm^3}{Nano^* s}$$

| Time (sec) | % Volume | Volume |
|---|---|---|
| 2928.3 | 0.00 | $3.37 \times 10^{-12}$ |
| 11713.6 | 18.18 | $2.76 \times 10^{-12}$ |
| 17570.3 | 38.64 | $2.07 \times 10^{-12}$ |
| 29283.9 | 45.00 | $1.85 \times 10^{-12}$ |
| 43926.0 | 52.73 | $1.59 \times 10^{-12}$ |
| 90780.2 | 61.36 | $1.30 \times 10^{-12}$ |
| 172775.3 | 77.73 | $7.50 \times 10^{-13}$ |
| 257698.8 | 85.45 | $4.90 \times 10^{-13}$ |
| 427545.5 | 91.36 | $2.91 \times 10^{-13}$ |
| 597392.5 | 92.27 | $2.60 \times 10^{-13}$ |

Table values were calculated using information taken from Siepmann and Gopferic. An exponential line was fit to the table values to produce the equation for $\frac{dVol}{dt}\frac{mm^3}{Nano^* s}$. The fitted regression line is shown with the best fit equation in Figure 23 below.

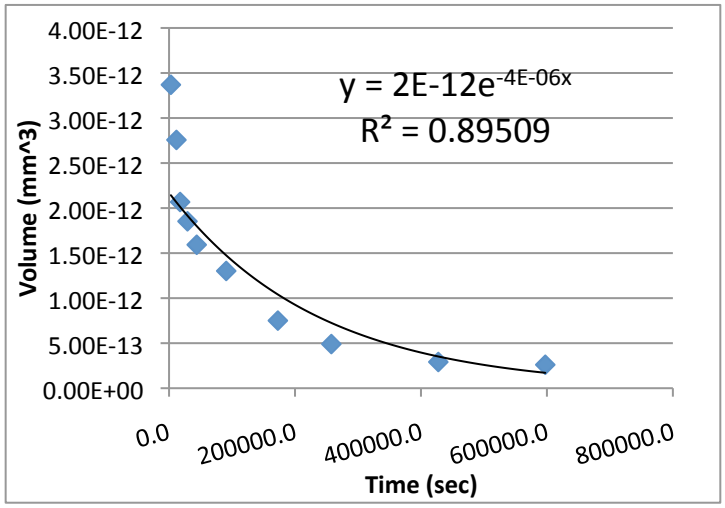


Figure 23: The volumetric degradation of the nanoparticle polymer with time. This graph shows how the polymer would decrease in volume as a function of the decided radius, releasing BCNU and allowing us to estimate the BCNU generation term as an exponential function with time.

**Drug degradation rate kc:**

$t_{1/2}$ = 0.52 hours = 1872 sec

$$k_C = \frac{\ln(2)}{1872\,\text{sec}} = 3.703 \times 10^{-4}\,\frac{1}{\text{sec}}$$

Only first order rate kinetics for all domains. [9]

**Number of nanoparticles in the wafer:**

$$Vol_{Nano} = \frac{4}{3}\pi r^3 = \frac{4}{3}\pi\left(\frac{186\times10^{-9}m}{2}\right)^3 = 3.36928\times10^{-21}m^3 = 3.36928\times10^{-12}mm^3$$

$$Vol_{Wafer} = (\pi r^2)(h) = \pi(\tfrac{14.5}{2}\times10^{-3}m)^2(1\times10^{-3}m) = 1.6513\times10^{-7}m^3$$

$$\#NanoWithinWaferHeight = \frac{WaferHeight}{NanoHeight} = \frac{(1\times10^{-3}m)}{186\times10^{-9}m} = 5376.34$$

$$\#NanoWithinWaferArea = \frac{WaferArea}{NanoDiameter} = \frac{\pi(14.5\times10^{-3}m)^2}{186\times10^{-9}m} = 3551.18$$

**Approximate that will only fill 4000 nanoparticles in wafer height, and 3000 in wafer area.**

$$Total\#NanoWithin1Wafer = (4000\times3000) = 12{,}000{,}000Nano$$

$$Total\#NanoWithin8Wafer = 8(12x10^6) = 96x10^6Nano$$

$$61.6mgBCNU\times\frac{8Wafers}{96x10^6Nano}\times\frac{1Nano}{3.36928x10^{-21}} = 1.90446\times10^{14}\ \tfrac{mgBCNU}{m^3Nano}$$

$$BCNU_{Generation} = \left(1.90446\times10^{14}\ \tfrac{mgBCNU}{m^3Nano}\right)\times\left(\tfrac{1m^3}{10^9mm^3}\right)\times\left(NanoPartDeg\ \tfrac{mm^3Nano}{nano*s}\right)\left(C_{Nano}\ \tfrac{Nano}{mm^3tissue}\right)$$

**Since the nanoparticles size is 186 ± 25 nm., if all the nanoparticles were to be around 161 nm., this is the calculation of how many can fit inside the wafer exactly. A maximum limit to the number of nanoparticles that can be placed in the wafer is:**

$$Vol_{Nano} = \frac{4}{3}\pi r^3 = \frac{4}{3}\pi\left(\frac{161\times10^{-9}m}{2}\right)^3 = 2.18512482\times10^{-21}m^3$$

$$Vol_{Wafer} = (\pi r^2)(h) = \pi(\tfrac{14.5}{2}\times10^{-3}m)^2(1\times10^{-3}m) = 1.6513\times10^{-7}m^3$$

$$\#NanoWithinWaferHeight = \frac{WaferHeight}{NanoHeight} = \frac{(1\times10^{-3}m)}{161\times10^{-9}m} = 6211.180124$$

$$\#NanoWithinWaferArea = \frac{WaferArea}{NanoDiameter} = \frac{\pi(14.5\times10^{-3}m)^2}{161\times10^{-9}m} = 4102.607798$$

Therefore, the approximation for the maximum amount of nanoparticles that could fit would be 6000 nanoparticles in the wafer height and 4000 in the wafer area.

**Size of tumor resurrected estimated by calculating the area that would be covered by 8 Gliadel wafers:**

$$A_{TopWafer} = \pi(7.25 \times 10^{-3})^2 = 1.6513 \times 10^{-4} m^2$$

$$A_{WaferTotal} = 8A_{TopWafer} = 8(1.6513 \times 10^{-4}) = 0.001321 m^2$$

$$A_{SemiCircle} = \frac{1}{2}(4\pi r_{Cavity}{}^2) = 2\pi r_{Cavity}{}^2$$

$$A_{WaferTotal} = A_{SemiCircle}$$

$$0.001321 m^2 = 2\pi r_{Cavity}{}^2$$

$$r_{Cavity} = 0.0145 m$$

**Number of nanoparticles for sensitivity analysis:**

12000000 (original), 14625000, 17500000, 20625000, 24000000

**Initial concentration of nanoparticles in wafer:**

$$\frac{\#Nano}{Vol_{Wafers}} = \frac{96x10^6}{8(1.6513x10^{-7})} = 7.267x10^{13} \frac{Nano}{m^3 wafer} = 7.267x10^4 \frac{Nano}{mm^3 wafer}$$

**For the maximum number of nanoparticles:**

$$Total\#NanoWithin1Wafer = (6000 \times 4000) = 24{,}000{,}000 Nano$$

$$Total\#NanoWithin8Wafer = 8(24{,}000{,}000) = 192000000 Nano$$

$$\frac{\#Nano}{Vol_{Wafers}} = \frac{192 \times 10^6}{8(1.6513 \times 10^{-7})} = 1.4534004E^{14} \frac{Nano}{m^3 wafer}$$

**Initial concentration of BCNU in wafer layer for accuracy check model to compare to clinical data for Gliadel wafers :**

$$\frac{BCNU}{Vol_{Wafers}} = \frac{61.6mg}{8(1.6513x10^{-7})} = 4.663x10^7 \frac{mg}{m^3 wafer} = 46.63 \frac{mg}{mm^3 wafer}$$

**Optimization value clow – clinically therapeutic level of BCNU necessary for antitumor effectiveness**

$$25.2\mu M \times \frac{1L}{10^6 mm^3} \times \frac{1mol}{10^6 \mu Mol} \times \frac{0.21405mg}{1mol} = 5.394x10^{-12} \frac{mg}{mm^3 tissue}$$

**Initial concentration of BCNU in wafer layer for no nanoparticle version to approximate cHigh for optimization:**

320 mg of BCNU total in wafers was the maximum amount where the side effects were consistent with lower amounts of BCNU total in the wafers- maximum threshold for BCNU in wafers

$$\frac{BCNU}{Vol_{Wafers}} = \frac{232mg}{8(1.6513x10^{-7})} = 17.562x10^{7} \frac{mg}{m^3 wafer}$$

320 mg of BCNU total in wafers caused cytotoxic effects and more extreme negative side effects

$$\frac{BCNU}{Vol_{Wafers}} = \frac{320mg}{8(1.6513x10^{-7})} = 24.223x10^{7} \frac{mg}{m^3 wafer}$$

## XI. Appendix C: Variables

Table 2: Values Used within COMSOL. The first column gives the name of the value, which describes the meaning of the variable. The variable column gives the variable as it was input and referred to within COMSOL. The third column gives the value or expression that corresponds to the variable listed in the second column. The source column gives the source from which the value was taken.

| Name | Variable | Value/ Expression | Source |
|---|---|---|---|
| Radius of Resurrected Tumor | $R_{cavity}$ | 14.5mm | [23] |
| Thickness of tumorous tissue not removed during surgery | $t_{tumor}$ | 3.1mm | [23] |
| Thickness of wafer layer | $t_{wafer}$ | 1.0mm | [21] |
| Molecular mass of BCNU | $MM_{BCNU}$ | $\frac{214.05g}{1mol}$ | [21] |
| Diffusivity of Nanoparticles | $D_{Nano}$ | $\frac{kT}{6\pi\eta r_{Nano}}$ | Stokes-Einstein Equation |
| Boltzman's Constant | K | $1.38065x10^{-17}\ \frac{kg\cdot mm^2}{s\cdot K}$ | Constant |
| Temperature | T | 315.15 K | [1] |
| Dynamic Viscosity | $\eta$ | $0.78x10^{-6}\ \frac{kg}{mm\cdot s}$ | [23] |
| Interstitial Fluid Density | $\rho$ | 1000 x $10^{-9}$ kg/mm$^3$ | [23] |
| Volume of Nanoparticle | $V_{Nano}$ | Variable | Calculation shown in Appendix B. |
| Radius of Nanoparticle | $r_{Nano}$ | $\left(\frac{3}{4\pi}V_{Nano}\right)^{\frac{1}{3}} mm$ | Formula for volume of a sphere |
| Diffusivity of BCNU in Cavity | $D_{BCNU\text{-}C}$ | $1.43x10^{-3}\ \frac{mm^2}{s}$ | [23] |
| Diffusivity of BCNU in Wafer | $D_{BCNU\text{-}W}$ | $2.00x10^{-6}\ \frac{mm^2}{s}$ | [23] |
| Diffusivity of BCNU in Tumorous Tissue | $D_{BCNU\text{-}T}$ | $6.75x10^{-3}\ \frac{mm^2}{s}$ | [23] |
| Diffusivity of BCNU in Normal Tissue | $D_{BCNU\text{-}N}$ | $2.5x10^{-4}\ \frac{mm^2}{s}$ | [23] |

| | | | |
|---|---|---|---|
| Half-Life of BCNU | $t_{1/2}$ | 0.52 hours | [1] |
| Changing Hydraulic Conductivity Parameter | $\chi$ | 4.583 x$10^{-3}$ 1/s | [23] |
| Hydraulic Conductivity of Microvascular wall in Tumor Tissue | $*K_v^T$ | $2.11x10^{-5}\ \frac{mm^2 \cdot s}{kg}$ | [23] |
| Hydraulic Conductivity of Microvascular wall in Normal Tissue | $*K_v^N$ | $2.7x10^{-6}\ \frac{mm^2 \cdot s}{kg}$ | [23] |
| Permeability of the Cavity | $K_{Br\text{-}C}$ | 1 x$10^{-5}$ $mm^2$ | [23] |
| Permeability of the Wafer | $K_{Br\text{-}W}$ | 3.01 x$10^{-7}$ $mm^2$ | [23] |
| Permeability of the Tumor Tissue | $K_{Br\text{-}T}$ | 6.4x$10^{-8}$ $mm^2$ | [9] |
| Permeability of Normal Tissue | $K_{Br\text{-}N}$ | 6.4x$10^{-9}$ $mm^2$ | [9] |
| Porosity of Wafer | $\varepsilon_W$ | 0.45 | [23] |
| Porosity of Cavity, Tumor, and Normal Tissue | $\varepsilon_C$<br>$\varepsilon_T$<br>$\varepsilon_N$ | 0.5 | [23] |
| Vascular Pressure | $P_V$ | 2.080 kPa | [23] |
| Pressure of Bulk Tissue | $P_{bulk}$ | 0.7992 kPa | [23] |
| Metabolism Rate Parameter | Q | $4.67x10^{-4}\ \frac{mm^3}{s \cdot kg}$ | [23] |
| Exchange area of blood vessels per unit of tumor tissue | $S/V^T$ | 20 mm | [23] |
| Exchange area of blood vessels per unit of normal tissue | $S/V^N$ | 7 mm | [23] |
| Osmotic reflection coefficient for BCNU in | $\sigma_T^T$ | 0.82 | [23] |

| | | | |
|---|---|---|---|
| tumor | | | |
| Osmotic reflection coefficient for BCNU in normal tissues | $\sigma_T^N$ | 0.91 | [23] |
| Osmotic pressure of plasma fluids | $\pi_v^T$<br>$\pi_v^N$ | 2.660 kPa | [23] |
| Osmotic pressure of interstitial fluids in tumor | $\pi_i^T$ | 2.000 kPa | [23] |
| Osmotic pressure of interstitial fluids in normal tissues | $\pi_i^N$ | 1.330 kPa | [23] |
| Clinically Therapeutic Level of BCNU | $c_{low}$ | 25.2 μM | [1] |

* - value changes with time. Supporting table below.

Table 3: $K_v$ values as they change with time. This term varies based on the time period of the edema and varies based on the location within the tumorous tissue or within the normal tissue. It is a measure of vascular permeability. The tissues take 6 hours to fill will fluid and drain with fluid. During the times of maximum edema, the $K_v$ is 100 times the baseline values. Baseline values are given in table 2 above.

| | | |
|---|---|---|
| $K_v^T$ | $2.11x\ 10^{-5}$ | $0<t<6$ hrs |
| | $2.11x10^{-5}(\chi t-98.0)$ | $6<t<12$ hrs |
| | $100(2.11x10^{-5})$ | $12 <t<36$ |
| | $2.11x10^{-5}(-\chi t+694)$ | $36<t<42$ |
| | $2.11x10^{-5}$ | $42<t<12$ days |
| $K_v^N$ | $2.7x10^{-6}$ | $0<t<6$ hrs |
| | $2.7x10^{-6}(\chi t-98.0)$ | $6<t<12$ hrs |
| | $100(2.7x10^{-6})$ | $12 <t<36$ |
| | $2.7x10^{-6}(-\chi t+694)$ | $36<t<42$ |
| | $2.7x10^{-6}$ | $42<t<12$ days |

# XII. Appendix D: Supplementary Graphs, Tables, and Figures

Table 1: Mesh Convergence Trials. Table 1 shows the concentrations of BCNU at times of 800000 seconds and 900000 seconds that were found on point graphs and each run at 2cm into the normal tissue. The number of elements was found through the statistics tab. However, the description and max element size determined this number of elements.

| DESCRIPTION | max element size | TOTAL NUMBER OF ELEMENTS | CONCENTRATION OF BCNU @ POINT (mg/mm^3) | |
|---|---|---|---|---|
| | | | 800000 | 900000 |
| extremely fine | 0.5 | 110944 | 0.00003 | 0.000078 |
| extremely fine | 0.75 | 50402 | 0.000033 | 0.000083 |
| extremely fine | 1 | 26632 | 0.000037 | 0.000088 |
| extra fine | 2 | 7702 | 0.000054 | 0.000103 |
| finer | 3.7 | 3314 | -5E-12 | 0 |

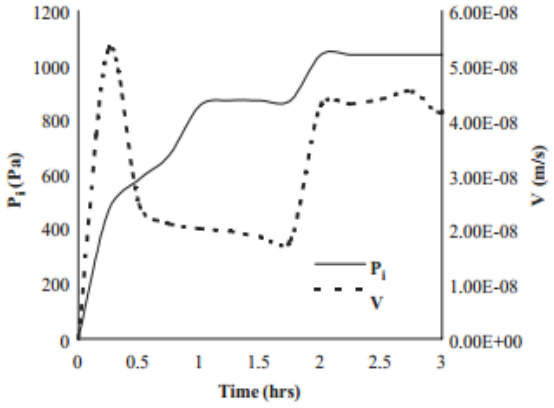


Fig. 3. Mean pressure ($P_i$) and fluid velocity ($V$) profile in cavity.

Figure 24: Cavity Pressure from Literature. The pressure is represented by the solid line and shows an increase in the cavity for the first the house. The pressure is initially at zero and then increases in step-like increments until a value of approximately 1000Pa is reached just after 2 hours

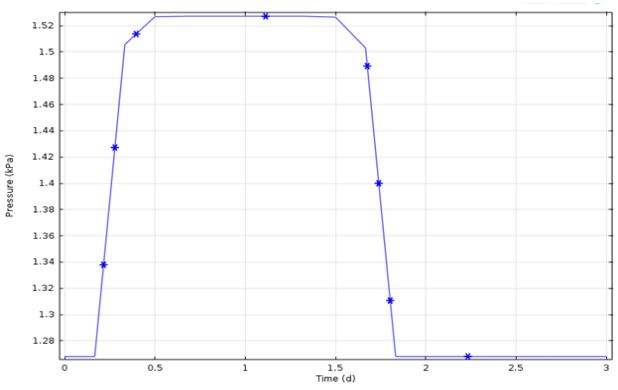


.

Figure 25: Cavity Pressure from Model. This shows the pressure over a three day time period, in comparison pressures from literature, which are in hours. It is steadily at a pressure of approximately 1.28 kPa for the three hour time period.

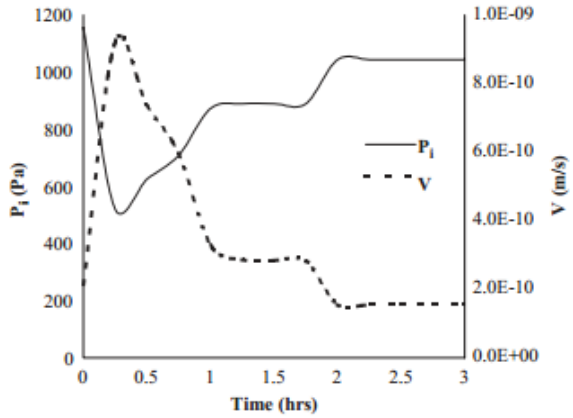


Fig. 7. Mean pressure ($P_i$) and fluid velocity ($V$) profile in the tumor.

Figure 26: Tumor Layer Pressure from Literature. Pressure is modeled by the solid line. It starts at 1200Pa then rapidly decline to about 500Pa within the first 0.5 hours. It then increases in step-like increments until a steady value of 1000Pa is reached around 2.25 hours.

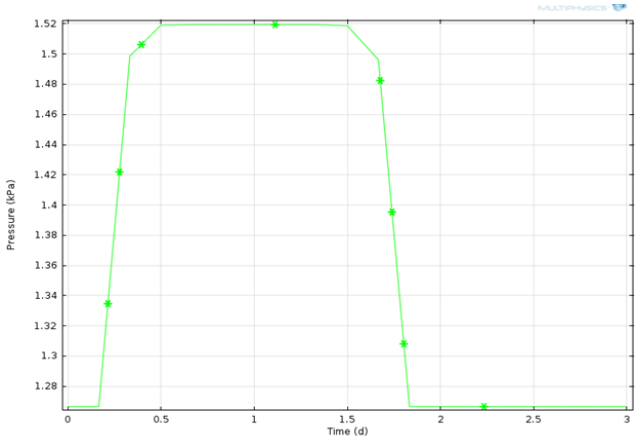


Figure 27: Tumor Layer Pressure from Model. This models pressure in the tumor layer over 3 days. In the first 3 hours, a steady line around 1.28 kPa is seen.

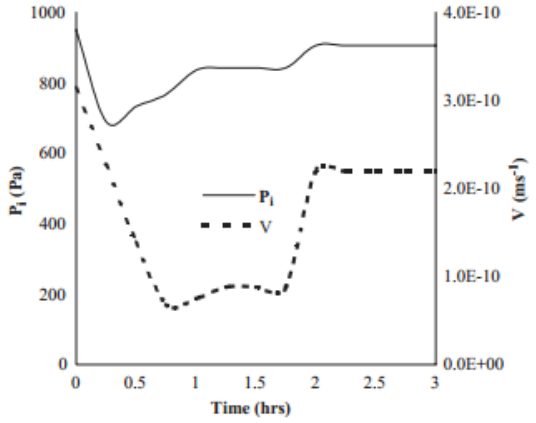


Fig. 10. Mean pressure ($P_i$) and fluid velocity ($V$) profiles in the tissues.

Figure 28: Normal Tissue Pressure From Literature. The solid line models the pressure in the normal tissue. It starts at 1000Pa then decreases to about 700Pa within the first 30 minutes. It increases in increments until a pressure of about 900Pa is reached at approximately 2.25 hours.

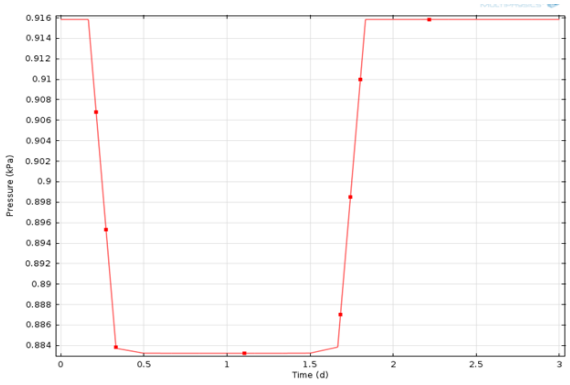


Figure 29: Normal Tissue Pressure from Model. This shows the pressure in the normal tissue over three days. In the first three hours, the pressure is at a constant value of approximately 0.915 kPa.

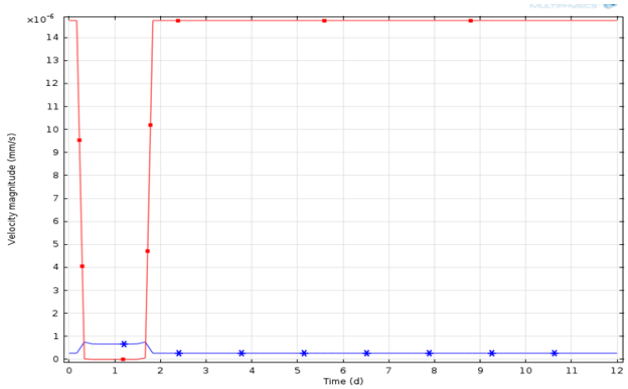


Figure 30: Velocity for Cavity (blue) and Normal Tissue (red). The velocity in the cavity remains at consistently low values of about 0.5 x $10^{-6}$ mm/s. The Normal tissue is initially steady at a value of about 14 x $10^{-6}$ mm/s for less than a day and then dips down to down 0.5 x $10^{-6}$ mm/s. At about day 2 it rises back to the value of 14 x $10^{-6}$mm/s.

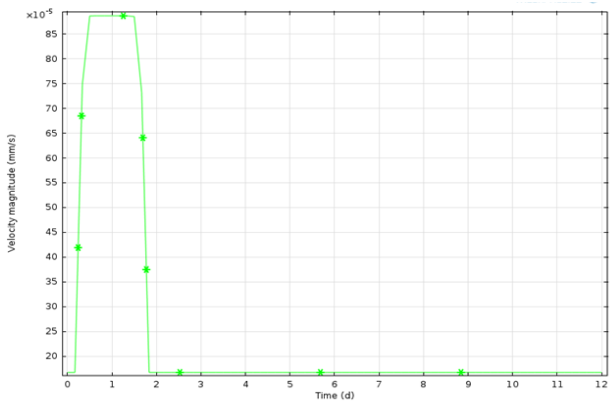


Figure 31: Velocity of Tumor Layer. The velocity in the tumor layer is initially at a low value and then peaks up to approximately 85 x $10^{-5}$mm/s after about half a day and remains at this velocity until about 2 days. Around 2 days it drops back down to this low initial value near zero.

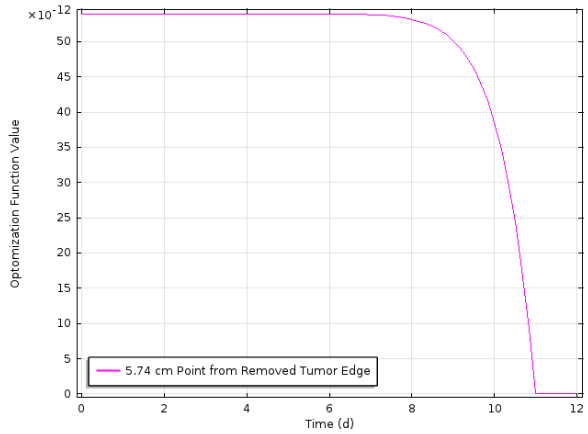


Figure 32: Penetration distance Curve. This figure shows the characteristic curve observed for distances within the normal tissue that were to be considered the maximum penetration distance. The maximum penetration distance was the distance at which this optimization curve was observed. There is a relatively constant value for the optimization for majority of the 12 days, but the distance reaches a therapeutic concentration, and hence optimization value, for the first time at day 11.

## IX. Appendix E: References


[1] Ali-Osman, Francis, Jane Giblin, and Dolores Daughtry. "Application of in Vivo and in Vitro Pharmacokinetics for Physiologically Relevant Drug Exposure in a Human Tumor Clonogenic Cell Assay." *Cancer Research* (1987): n. pag. Web. 18 Apr. 2013.

[2] Bodell, William J., Alexander P. Bodell, and Donald D. Giannini. "Levels and Distribution of BCNU in GBM Tumors following Intratumoral Injection of DTI-015 (BCNU-ethanol)." *Society for Nuero-Onocology* (2006): n. pag. Web. 18 Apr. 2013. <http://www.ncbi.nlm.nih.gov/pmc/articles/PMC1828109/pdf/neu0901p012.pdf>.

[3] Bota, Daniela A., Annick Desjardins, Jennifer A. Quinn, Mary L. Affronti, and Henry S. Friedman. "Interstitial Chemotherapy with Biodegradable BCNU (Gliadel®) Wafers in the Treatment of Malignant Gliomas." *The Clin Risk Manag.* (2007): 707-15. Web. 18 Apr. 2013. <http://www.ncbi.nlm.nih.gov/pmc/articles/PMC2376068/>.

[4] Brem, H., S. Piantadosi, P. C. Burger, M. Walker, R. Selker, N. A. Vick, K. Black, M. Sisti, S. Brem, G. Mohr, P. Muller, R. Morawetz, and S. C. Schold. "Placebo-controlled Trial of Safety and Efficacy of Intraoperative Controlled Delivery by Biodegradable Polymers of Chemotherapy for Recurrent Gliomas." *Science Direct* 345.8946 (n.d.): 1008-012. Web. 18 Apr. 2013. <http://www.sciencedirect.com/science/article/pii/S0140673695907556>.

[5] "Carmustine." *The Scott Hamilton CARES Initiative- Drug Information*. N.p., n.d. Web. 18 Apr. 2013. <http://chemocare.com/chemotherapy/drug-info/carmustine.aspx>.

[6] "Cerebrospinal Fluid (CSF) (anatomy)." *Encyclopedia Britannica Online*. Encyclopedia Britannica, n.d. Web. 18 Apr. 2013. <http://www.britannica.com/EBchecked/topic/103430/cerebrospinal-fluid-CSF?anchor=ref22476>.

[7] Cooney, David O. "Effect of Geometry on the Dissolution of Pharmaceutical Tablets and Other Solids: Surface Detachment Kinetics Controlling." *AlCHE Journal* 2nd ser. 18 (n.d.): n. pag. Web. 18 Apr. 2013. <https://dl-web.dropbox.com/get/Group06/Cooney%20Paper%20on%20Dissolution.pdf?w=AABp9_OL1m3DblfmRILkA6UnlmNddVGxtI0PB77tmvlnjg>.

[8] Erickson, William L., Lyndsey Fortin, Cheryl Hou, and Katrina Shum. *Drug Delivery via GLIADEL Wafer for Treatment of Glioblastoma Multiforme (GBM)*. N.p., 2008. Web. 18 Apr. 2013. <http://dspace.library.cornell.edu/bitstream/1813/11132/1/Group%205.pdf>.

[9] Fleming, Alison B., and W. M. Saltzman. "Pharmacokinetics of the Carmustine Implant." (2002): n. pag. Web. 18 Apr. 2013. <https://dl-web.dropbox.com/get/Group06/Pharmacokinetics%20of%20Carmustine%20Implant.pdf?w=AABEONEcdVl34Ie88l38Vg9YNhpUy8iiSzMTid_hXvHdGg>.

[10] Gasper, Lauire E., Barbara J. Fisher, David R. MacDonald, Deborah B. Leber, Edward C. Halperin, S. Clifford Schold, Jr., and Gregory Cairncross. "Supratentorial Malignant Glioma: Patterns of Recurrence and Implications for External Beam Local Treatment."

*Science Direct* 24.1 (n.d.): n. pag. Web. 18 Apr. 2013. <http://www.sciencedirect.com/science/article/pii/036030169291021E>.

[11] Guido, Fronsina. "DNA Repair and Resistance of Gliomas to Chemotherapy and Radiotherapy." *DNA Repair and Resistance of Gliomas to Chemotherapy and Radiotherapy*. N.p., n.d. Web. 7 Mar. 2013.

[12] Hou, Lewis C., Anand Veeravagu, Andrew R. Hsu, and Victor C. K. Tse. "Recurrent Glioblastoma Multiforme: A Review of Natural History and Management Options."*Neurosurgical FOCUS* 20.4 (2006): E3. Web.

[13] Lassen, U., P. E. Kristjansen, A. Wagner, M. Kosteljanetz, and J. S. Poulsen. "Treatment of Newly Diagnosed Glioblastoma Multiforme with Carmustine, Cisplatin and Etoposide Followed by Radiotherapy. A Phase II Study." *National Center for Biotechnology Information*. U.S. National Library of Medicine, n.d. Web. 18 Apr. 2013. <http://www.ncbi.nlm.nih.gov/pubmed/>.

[14] Lee, Wen- Chuan, and Ming Chu. "Preparation and Degradation Behavior of Polyanhydrides Nanoparticles." (2007): n. pag. Web. 18 Apr. 2013. <https://dl-web.dropbox.com/get/Group06/anhydride%20nanoparticle.pdf?w=AACn5HZCRU_5RMgw0FlSiCDVdgOWEDY5XorWGN8BXm3PMg>.

[15] Loo, Ti Li, Robert L. Dion, Robert L. Dixon, and David P. Rall. "The Antitumor Agent, 1,3-Bis( 2 -chloroethyl)-1-nitrosourea." *Wiley Online Library* 55.5 (2006): n. pag. Web. 18 Apr. 2013. <http://onlinelibrary.wiley.com/doi/10.1002/jps.2600550509/pdf>.

[16] *Medscape*. N.p., n.d. Web. 18 Apr. 2013. <http://www.medscape.com/viewarticle/540150_2>.

[17] Melvin, J. W., G. T. Fallenstein, and V. D. Hulce. "DYNAMIC MECHANICAL PROPERTIES OF HUMAN BRAIN TISSUE." *J. Biomechanics* 202 (n.d.): 217-26. Web. 18 Apr. 2013. <https://dl-web.dropbox.com/get/Group06/brain%20viscosity.pdf?w=AACfFDrg0-fK0w8gwMEeNWgVtIdsF4JQgTP6GREmdkmiJA>.

[18] Nagashima, Tatsuya, Takayuki Shirakuni, and Stanley I. Rapoport. "A Two-dimensional, Finite Element Analysis of Vasogenic Brain Edema." *Neurol Med Chir* 30 (1990): 1-9. Web. 18 Apr. 2013.

[19] Olivi, Alessandro, Stuart A. Grossman, Stephan Tatter, Fred Barker, Kevin Judy, Jeffery Olsen, Jeffery Bruce, Dana Hilt, Joy Fisher, and Steven Piantados. "Dose Escalation of Carmustine in Surgically Implanted Polymers in Patients With Recurrent Malignant Glioma: A New Approaches to Brain Tumor Therapy CNS Consortium Trial." (2003): n. pag. *American Society of Clinical Oncology*. Web. 18 Apr. 2013.

[20] "Pros and Cons of GMOs." *LoveToKnow*. N.p., n.d. Web. 14 Apr. 2013. <http://organic.lovetoknow.com/Pros_and_Cons_of_GMOs>.

[21] "Resource Center." *Gliadel*. Gliadel, 2013. Web. 18 Apr. 2013. <http://www.gliadel.com/hcp/resources/>.

[22] Siepmann, J., and A. Gopferich. "Mathematical Modeling of Bioerodible, Polymeric Drug Delivery Systems." (2001): 229-47. Web. 18 Apr. 2013. <https://dl-web.dropbox.com/get/Group06/math%20modeling%20of%20surface%20erosion.pdf?w=AADPsXug1KythAUfidFutjCIXGT1tkewxJKZRSTOVF57HA>.

[23] *Transient Interstitial fluid flow in Brain Tumors: Effect on Drug Delivery* 60 (2005): 4803-821. *Elsevier*. Web. 18 Apr. 2013. <https://dl-web.dropbox.com/get/Group06/Transient%20interstitial%20flow%20in%20brain.pdf?w=AAATYZhvvTN1gK-dRCoyhUoT4mcA1gBC1PtyVoz27ac7Yw>.

[24] "Types of Brain Cancer." *CTCA Cancer Treatment Centers & Hospitals*. N.p., n.d. Web. 18 Apr. 2013. <http://www.cancercenter.com/brain-cancer/types-of-brain-cancer.cfm?OVMTC=Phrase>.

[25] "Types of Gliomas." *Johns Hopkins Medicine, Based in Baltimore, Maryland*. N.p., n.d. Web. 18 Apr. 2013. <http://www.hopkinsmedicine.org/neurology_neurosurgery/specialty_areas/brain_tumor/center/glioma/types/index.html>.

[26] Fung, L. K., Ewend, M. G., Sills, A., & et al., (1998). Pharmacokinetics of interstitial delivery of carmustine, 4-hydroperoxycyclophosphamide, and paclitaxel from a biodegradable polymer implant in the monkey brain. *Cancer Research*, *58*(4), 672-684.